# Coherent lattice dynamics in topological insulator $Bi_2Te_3$ probed with time-resolved optical second-harmonic generation

Anton Y. Bykov* and Tatiana V. Murzina
*Department of Physics, Moscow State University, 119991 Moscow, Russia*

Nicolas Olivier, Gregory A. Wurtz, and Anatoly V. Zayats
*Department of Physics, King's College London, Strand, London WC2R 2LS, United Kingdom*
(Received 30 April 2015; revised manuscript received 28 June 2015; published 28 August 2015)

The dynamics of phonon modes in thin flakes of topological insulator $Bi_2Te_3$ has been studied using transient optical second-harmonic spectroscopy. Using the surface sensitivity of second-harmonic generation, the excitation and dynamics of a family of optical phonon modes are observed with a response dependent on the excitation polarization. Three coherent phonon modes, inaccessible in previous linear time-resolved optical measurements, were detected in the nonlinear dynamic response. A symmetry-allowed *surface* optical phonon mode in $Bi_2Te_3$ has been identified using surface and symmetry selectivity of the second-order up-conversion process. Possible second-harmonic generation mechanisms in $Bi_2Te_3$ as well as the enhanced sensitivity of the nonlinear processes for the phonon mode detection in topological insulators are discussed.

DOI: 10.1103/PhysRevB.92.064305 PACS number(s): 78.47.D−, 63.20.D−, 68.35.Ja, 78.66.−w

Topological insulators (TIs) are a family of materials with specific topological order which allows for the surface conducting states protected by time-reversal symmetry, being insulators in the bulk [1]. While electron behavior in TIs has been studied in detail, electron-phonon interactions at the surface of topological insulators are less understood. This however is of particular importance since for high-quality crystals, electron-phonon interaction represents a dominant scattering mechanism that limits possible applications in electronic and spintronic devices. On the other hand, it also carries information on fundamental electronic properties of the topological insulator [2–5]. The appearance of the IR-active mode in the Raman scattering has been reported in few-QL films due to the symmetry breaking [7]. The coupling of a bulk phonon mode to the surface states arising from reduction of the interlayer van der Waals forces near the surface have also been found using angle-resolved photoemission spectroscopy [6]. All these studies of phonon and electron-phonon processes at a TI surface require optical characterization techniques with high surface sensitivity.

In this respect, optical second-harmonic generation (SHG) is one of the most ubiquitous methods in surface science with extraordinary surface sensitivity [8]. SHG provides selective probing of surfaces and buried interfaces since it is forbidden, in the electric dipole approximation, from the bulk of centrosymmetric materials due to symmetry considerations. High sensitivity to possible sources of external symmetry breaking such as fields and strain is also beneficial for studies of defects and interfacial electric fields in semiconductor heterostructures or domains in ferromagnetic and ferroelectric materials [9,10]. In particular, time-resolved second-harmonic generation measurements can be used to probe electron and lattice dynamics of surface and thin layers of materials [11,12], including topological insulator $Bi_2Se_3$ [13,14].

Bismuth telluride ($Bi_2Te_3$) is a topological insulator and a narrow-band semiconductor material. High surface electric conductivity and low lattice thermal conductivity of $Bi_2Te_3$ determine a high thermoelectric figure of merit up to 1 and makes it ideal for applications in thermoelectric functional devices [15]. Bismuth telluride crystals have a rich spectrum of phonon modes previously observed with Fourier transform infrared (FTIR) and Raman spectroscopies (incoherent modes) [16,17] as well as pump-probe reflectivity spectroscopy in the visible spectral range (coherent phonon modes, excited by an ultrafast optical pump) [18–20]. The phonon spectrum of $Bi_2Te_3$ crystals contains 15 vibrational modes that are classified as 3 acoustic and 12 optical phonon modes, out of which only eight are nondegenerated, namely 4 Raman-active ($A_{1g}$, $E_g$) and 4 IR-absorption-active modes ($A_{2u}$, $E_u$). Hereafter, we use the group theoretical notation, so that the mode referred to as $A_{1u}$ in a number of experimental studies [16,18,19] is $A_{2u}$ in our notation. Among these modes, only the longitudinal $A_{1g}$ modes and $E_u^2$ modes have been observed in femtosecond pump-probe reflection measurements, with other modes known from infrared absorption and Raman studies. Coherent transverse phonon modes might have also been excited in the pump-probe experiments, but their detection is far more challenging than that of longitudinal modes. In order to detect transverse phonon modes, phonon-induced anisotropy in the material should be measured.

Unlike reflectivity dynamics, which is commonly measured with conventional pump-probe spectroscopy techniques, SHG is intrinsically sensitive to the symmetry of an anisotropic medium, and, thus, it can be directly applied to the investigation of transverse phonon modes. Surface phonon modes have not been identified in the previous studies of $Bi_2Te_3$, which are important for the understanding of electron scattering processes in these materials.

In this paper, we report an experimental investigation of optical phonon modes in thin flakes of the topological insulator bismuth telluride ($Bi_2Te_3$) using femtosecond time-resolved second-harmonic generation. We show that the transient SHG allows the visualization, in addition to electronic dynamics, of a family of $Bi_2Te_3$ phonon modes, including transverse phonon modes. Polarization selectivity in both phonon excitation and

*lancaster@shg.ru

 

detection allowed identifying several coherent phonon modes and observing dipole-allowed surface phonon modes in the topological insulator $Bi_2Te_3$. Symmetry analysis of the SHG process was carried out in order to understand the underlying mechanism of the excitation of various coherent phonon modes.

Thin flakes of $Bi_2Te_3$ were produced by mechanical exfoliation of high-quality single crystals grown by the Bridgman method onto 150 $\mu$m thick glass cover slides. Typical thickness of the produced flakes was around 50 nm (about 50 quintuple layers), as determined by AFM studies.

For the time-resolved pump-probe spectroscopy, light from an optical parametric amplifier (OPA) pumped by the output of an amplified Ti:sapphire laser was used as the fundamental beam to generate the second-harmonic light in reflection from the sample. The fundamental beam was set to a 1300 nm wavelength and 150 fs pulse width, with a fluence below 0.05 mJ/cm$^2$. The ultrafast transient changes in the SHG intensity were monitored as a probe of electron dynamics under the illumination of a control (pump) beam of 800 nm wavelength and 70 fs pulse width. Both beams were weakly focused onto the sample at about 30° incidence with a 40× reflective objective, into a focal spot approximately 40 $\mu m$ in diameter. In all experiments, the input fluence for the control beam was chosen just below the damage threshold of the material to ensure the highest reproducible differential SHG signal. The reflected second-harmonic light at 650 nm was collected with the same objective, spectrally selected by a set of interference short-pass filters, and detected with the imaging spectrograph.

Bismuth telluride is a centrosymmetric layered compound with a unit cell composed of five alternating Bi and Te layers [16] and which possesses $R\bar{3}m$ ($D_{3d}$) symmetry. Therefore, it is not expected to produce any SHG from the bulk. However, since the surfaces of $Bi_2Te_3$ layers have a (111) crystal symmetry, an anisotropic dipole surface SHG is allowed even at normal incidence, governed by the second-order susceptibility components $\chi_{xxx} = -\chi_{xyy} = -\chi_{yyx} = -\chi_{yxy}$ [21], where the $x$ and $y$ axes are in the flake surface plane. For oblique illumination, an additional $z$ component appears in the second-order susceptibility tensor due to the symmetry breaking at the surface.

The measured $Bi_2Te_3$ thin flakes exhibit strong SHG in reflection. Azimuthal SHG intensity dependencies, measured at normal incidence (not shown), are consistent with the (111) surface symmetry. For the time-resolved measurements, the samples were oriented so as to ensure maximum SHG signal for a given combination of the fundamental and SH light polarizations. Figure 1 shows the typical pump-probe dependencies of the reflected SHG intensity, $I_{2\omega}(\tau)$, obtained with different polarizations of the pump beam. As can be seen from the inset in Fig. 1, the SHG time dependence $I_{2\omega}(\tau)$ is biexponential with the time constants $\tau_1 \approx 2 \pm 0.2$ ps and $\tau_2 \approx 68 \pm 23$ ps, as extracted from the fit of the experimental data. These time constants are attributed to the dynamics of free carriers excited into unoccupied states of the surface and bulk electron bands, respectively [22]. A strong periodic modulation of the SHG intensity on the picosecond time scale reveals phonon contributions in the electron dynamics.

The crystal lattice dynamics manifests itself by series of optical phonon modes, whose excitation efficiency is

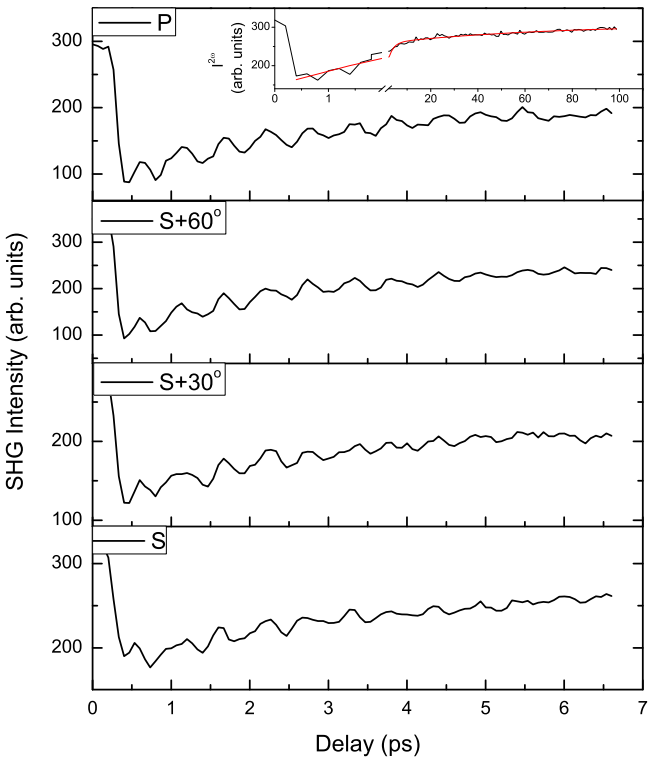


FIG. 1. (Color online) Time-resolved SHG signal for different polarizations of the control beam. $S$-polarized SHG was measured with the $S$-polarized fundamental light. Inset shows the SHG kinetics on large time scale.

sensitive to the polarization of the pump beam (Fig. 2). In the $S_\omega$-$S_{2\omega}$ polarization configuration, the most intense phonon line observed in the transient SHG spectra is close to 1.82 THz, a frequency at which the $A^1_{1g}$ phonon mode is usually observed in the (linear) reflectivity pump-probe measurements. The feature observed at about 2.8–2.9 THz corresponds to $A^1_{2u}$ and $E^2_u$ phonons, which have close frequencies and cannot be resolved in our measurements. (Please note that in some papers $A_{2u}$ modes are designated as $A_{1u}$ ones.) As can be seen from comparison of Figs. 2(a) and 2(b), the relative amplitude of the peaks $I_{2.85THz}/I_{1.82THz}$ depends on the polarization of the pump beam [Fig. 2(c)]. In fact, the ratio $I_{2.85THz}/I_{1.82THz}$ is 2.5 times larger for an $S$-polarized pump light compared to a $P$-polarized one. This dependence neither bears the signature of the threefold symmetry of the $Bi_2Te_3$ surface nor depends on the angle between the polarizations of the pump and the fundamental light, as evidenced from the cross-polarized fundamental/SHG measurements.

For a $P$-polarized fundamental light ($P_\omega$-$S_{2\omega}$ polarization configuration), the third phonon mode appears at around 1.5 THz, which is close to the predicted frequency of the $E^1_u$ IR-active phonon mode (Fig. 3).

The extensive polarization dependence for this mode has not been carried out. However, based on the results shown in Figs. 3(a) and 3(b), it is believed that the polarization dependence of this mode on the polarization of the pump has the opposite behavior compared to the $A^1_{2u}$ mode observed before. Interestingly, the high-energy phonon mode $A^2_{1g}$ at 3.9 THz has not been detected in our SHG measurements. This

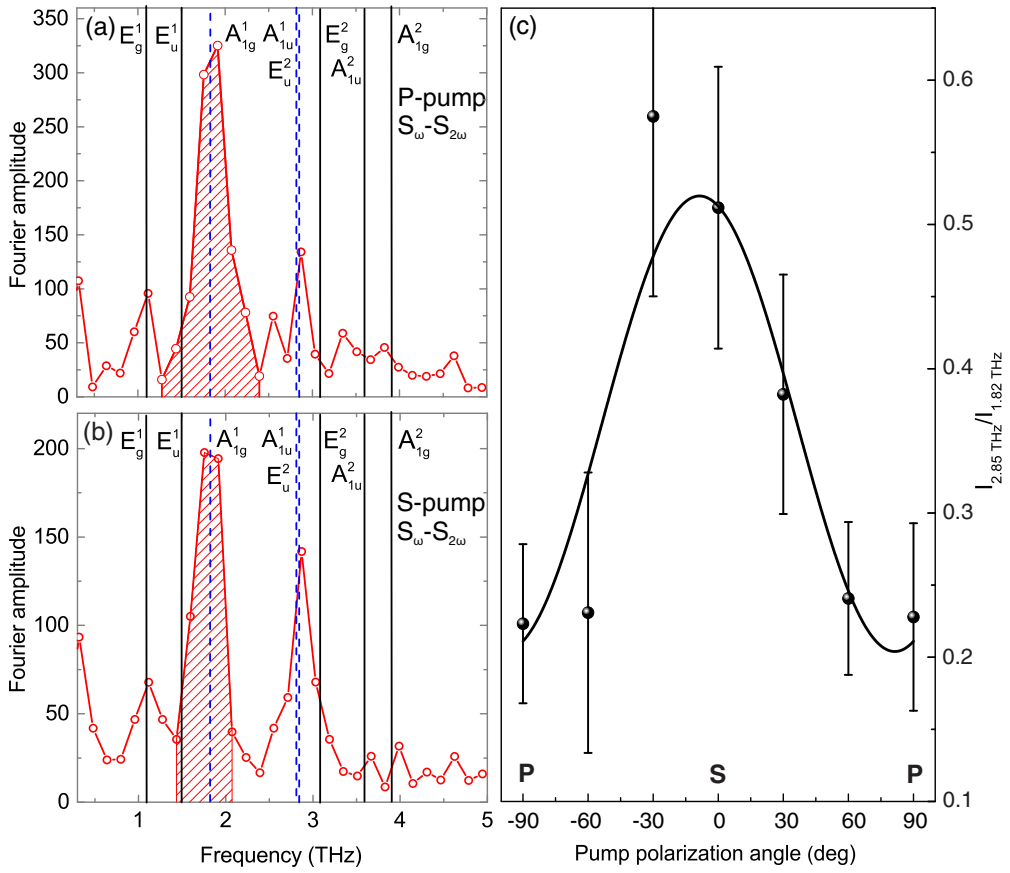


FIG. 2. (Color online) Fourier spectra of the time-resolved SHG intensity from $Bi_2Te_3$ flakes in $S_\omega$-$S_{2\omega}$ polarization configuration, measured for (a) *P*- and (b) *S*-polarized pump. Dashed lines indicate the phonon modes observed in the measurements. Solid lines indicate the phonon modes observed in [16,17]. Dashed area represents the $A_1$ surface mode. (c) Dependence of the relative contribution of two phonon modes $I_{2.85THz}/I_{1.82THz}$ on the polarization of the pump. Zero angle corresponds to the *S*-polarized pump.

mode has been reported to emerge at high fluencies in all linear reflectivity pump-probe measurements [18–20]. Despite the pump fluence in the SHG time-resolved measurements (about 1 mJ/cm$^2$) being set just below the material damage threshold and exceeding significantly those used in the previous linear studies, the $A^2_{1g}$ phonon mode has not been observed in the transient SHG signal. Similarly, the high-frequency modes (indicated with "2" superscript) from each pair of $A^{1,2}_{1g}$, $A^{1,2}_{2u}$,

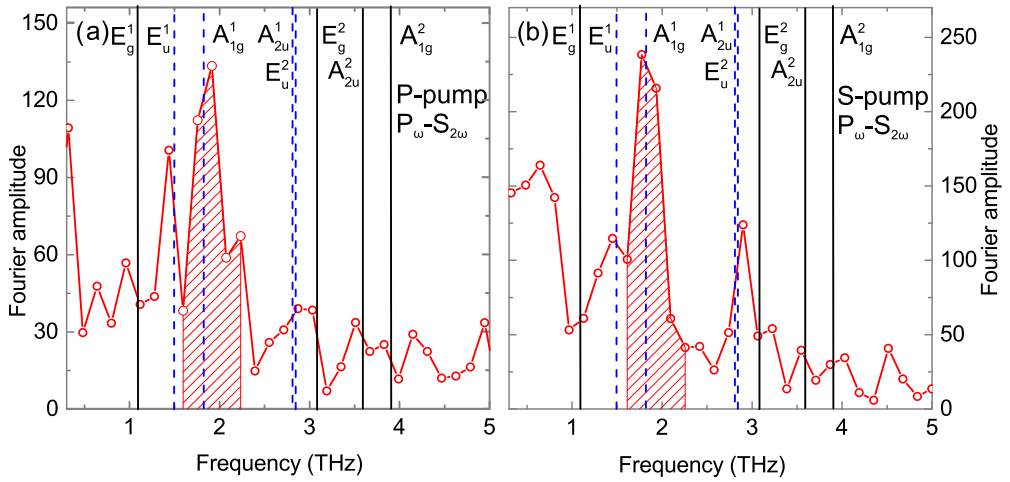


FIG. 3. (Color online) Fourier spectra of the time-resolved SHG intensity from $Bi_2Te_3$ flakes in $P_\omega$-$S_{2\omega}$ polarization configuration, measured for (a) *P*- and (b) *S*-polarized pump. Dashed lines indicate the phonon modes observed in the measurements. Solid lines indicate the phonon modes observed in [16,17]. Dashed area represents the $A_1$ surface mode.

TABLE I. Nonzero bulk $\chi^{(2)}_{ijk}$ susceptibility components.

| Mode | $ijk$ |
|---|---|
| $A_{2u}$ | $xxx = -xyy = -yyx, yyz = zyy = zxx = xxz, zzz$ |
| $E_u(x)$ | $xxx = 3xyy = 3yyx, xyz = yxz = zyx, zzx = xzz$ |
| $E_u(y)$ | $yyy = 3xxy = 3yxx, yyz = zyy = -zxx = -xxz, yzz = zzy$ |

$E^{1,2}_{1g}$, and $E^{1,2}_{u}$ were not observed in the SHG measurements either.

The mechanism determining the contribution of phonons to the SHG response is the local breaking of the crystal lattice symmetry due to the pump-induced movement of atoms away from their equilibrium positions. From a phenomenological point of view, the symmetry analysis required to explain the time-dependent SHG due to the lattice vibrations is equivalent to that conventionally performed for second-order hyper-Raman scattering [23]. For a given point symmetry group, lattice vibrations are classified with respect to irreducible representations of the group. Taking the character table for the point group ($D_{3d}$ in our case) that contains the symmetry of the different phonon modes with respect to the elementary symmetry operations such as identity, inversion, mirror planes, and rotation axes, one can obtain nonzero components of the polarizability tensor of the required order. The second rank (first order) tensor governs linear Raman scattering as well as the reflectivity changes in the linear pump-probe studies, while the second-order (third-rank) tensor is responsible for hyper-Raman and transient SHG. Considering $Bi_2Te_3$ bulk and surface point symmetry groups [24], nonvanishing $\chi^{(2)}$ tensor elements induced by various modes can be evaluated (Tables I and II).

Nonvanishing second-order susceptibility components for the bulk of $Bi_2Te_3$ with $D_{3d}$ symmetry are shown in Table I. Here the $x$ axis coincides with the direction of the electric field for the $S$-polarized fundamental and SH light and is orthogonal to the $C_2$ rotation axis in the plane of the flake, in accordance with the experimental geometry. As seen from Table I, both $E_u$ and $A_{2u}$ modes have nonzero $\chi_{xxx}$, $\chi_{xyy}$ components, which explains why they are observed in both $S_\omega$-$S_{2\omega}$ and $P_\omega$-$S_{2\omega}$ combinations of polarizations.

At the surface, the symmetry is reduced to $C_{3v}$ so that the total number of phonon modes is reduced to 2, both of which are now active in the second-harmonic response. For these modes, similar symmetry group derivations can be performed to determine nonvanishing susceptibility tensor components (Table II). As can be seen from Table II, the $A_1$ surface mode is observable in the $S$-polarized SHG. $E$ modes are also allowed but cannot be separated from the bulk phonon modes as they have the same symmetry and presumably close frequencies.

Raman-active phonon modes, designated by "g" (Figs. 2, 3), are symmetric with respect to inversion, making them impossible to be observed in the second-harmonic response from the bulk. Nevertheless, they are detected in our experiments due to the $C_{3v}$ symmetry of the (111) $Bi_2Te_3$ surface, which reduces the number of possible surface modes, making them observable in the nonlinear-optical response. Therefore, the strongest phonon mode at around 1.8–1.9 THz is identified as the $A_1$ surface mode, rather than the bulk $A^1_{1g}$ mode. The absence of the $A^2_{1g}$ mode at 4 THz, which is commonly observed together with its lower-energy counterpart $A^1_{1g}$, is, therefore, the result of the symmetry reduction, since this mode is no longer present on a surface. To the best of our knowledge, the *surface* phonon mode has not been observed previously in $Bi_2Te_3$, while the IR-active bulk phonon modes that are always active in hyper-Raman response were expected in the SHG spectra as well. Considering the crystal symmetry, the two remaining observed modes can be either surface or bulk ones, which have close frequencies and are both allowed due to symmetry considerations (Tables I, II). However, since bulk phonon modes are no longer forbidden in the electric dipole approximation, it is expected that the bulk contribution is dominant.

The dependence of the relative amplitudes of the SHG-visualized modes on the polarization of the pump can be understood within the scope of the displacement excitation of coherent phonons (DECP)/impulsed stimulated Raman scattering (ISRS) [25,26] theory. Due to the symmetry breaking, the $A_1$ mode is no longer exclusively IR or Raman active and can be excited more efficiently for $P$-polarized pump than for $S$-polarized pump, as larger numbers of components of the Raman tensor are involved in that case. The opposite dependence for the transverse mode can be attributed to the same process for the surface $E$ mode that contributes to the overall signal at the frequency of the $E_u$ and may have the opposite dependence on the polarization of the pump beam for some values of the Raman tensor components due to a more complicated dependence on their combination. It however remains unclear, purely from the symmetry considerations, why the $E/E_u$ mode is only observed in the $P_\omega$-$S_{2\omega}$ polarization configuration and not in the $S_\omega$-$S_{2\omega}$ one. This may be due to the dominant contribution of $\chi^{(2)}_{xzz}$ susceptibility component in the (111) $Bi_2Te_3$ flakes, compared to the $\chi^{(2)}_{xxx}$.

TABLE II. Nonzero surface $\chi^{(2)}_{ijk}$ susceptibility components.

| Mode | $ijk$ |
|---|---|
| $A_1$ | $xxx = -xyy = -yyx, yyz = zyy = zxx = xxz, zzz$ |
| $E(x)$ | $xxx = 3xyy = 3yyx, yyz = zyy = -zxx = -xxz, zzx = xzz$ |
| $E(y)$ | $yyy = 3xxy = 3yxx, xyz = yxz = zyx, yzz = zzy$ |

An alternative source of the symmetry breaking which can also contribute to the SHG observations may in principle be related to a built-in electric field due to the near-surface band bending that is known to contribute to the SHG in semiconductors, including topological insulators [13]. In the latter case, the electric field pointing towards the surface breaks the inversion symmetry and reduces Raman active bulk $A^1_{1g}$ mode to hyper-Raman active bulk $A^1$ mode. In our study, this effect cannot be distinguished from the symmetry breaking associated with the presence of the surface as it yields the same set of susceptibility tensor components and requires further investigations.

In conclusion, we have studied the excitation and dynamics of optically induced phonon modes in ultrathin bismuth telluride crystals using transient second-harmonic generation. Optically induced dynamics of optical phonons in $Bi_2Te_3$ studied by this technique reveals a clear dependence on the polarization of the pump radiation. Together with the SHG polarization dependencies, this allows a classification of phonon modes of the topological insulator. Two coherent IR-active phonon modes ($E^1_u$ and $A^1_{2u}$) were detected using transient SHG that have so far been inaccessible in previous linear time-resolved optical measurements [18–20]. No modulation of the SHG intensity was observed at the frequencies corresponding to the bulk Raman-active modes $E^{1,2}_g$ and $A^2_{1g}$ in agreement with our symmetry considerations. Moreover, the surface and symmetry selectivity of the second-order up-conversion process allowed observation of an $A_1$ optical phonon in $Bi_2Te_3$ attributed to either symmetry breaking at the surface or internal electric-field-induced symmetry breaking. The presented results are important for understanding fundamental electron-phonon interactions in topological insulators and their possible applications in electronic and spintronic devices. In a recent paper [27], Glinka *et al.* reported the enhancement of the SHG in $Bi_2Se_3$ driven by the excitation of a Dirac plasmon via inverse Raman process for the Raman-active surface mode. As confirmed by their previous Raman studies [28], the excitation is achieved through the use of quantum interference between the surface states and the surface optical phonon. Even though such quantum interference has not been observed yet in $Bi_2Te_3$, we believe similar effects can occur involving surface phonons observed in this work.

The authors thank Prof. Lada Yashina for providing $Bi_2Te_3$ single crystals, Sandro Minguzzi for assistance in preparing exfoliated samples, and Prof. Oleg Misochko for helpful discussions. This work has been supported, in part, by EPSRC (UK). A.B. was supported by the ESF Plasmon-Bionanosense network exchange visit grant. G.W. acknowledges support from EC FP7 Project No. 304179 (Marie Curie Actions). A.Z. acknowledges support from the Royal Society and the Wolfson Foundation. Partial support from RFBR, Grant No. 13-02-01102, is acknowledged.

[1] C. L. Kane and E. J. Mele, Phys. Rev. Lett. **95**, 146802 (2005).
[2] X. Zhu, L. Santos, C. Howard, R. Sankar, F. C. Chou, C. Chamon, and M. El-Batanouny, Phys. Rev. Lett. **108**, 185501 (2012).
[3] V. Parente, A. Tagliacozzo, F. von Oppen, and F. Guinea, Phys. Rev. B **88**, 075432 (2013).
[4] Z.-H. Pan, A. V. Fedorov, D. Gardner, Y. S. Lee, S. Chu, and T. Valla, Phys. Rev. Lett. **108**, 187001 (2012).
[5] R. C. Hatch, M. Bianchi, D. Guan, S. Bao, J. Mi, B. B. Iversen, L. Nilsson, L. Hornekær, and P. Hofmann, Phys. Rev. B **83**, 241303 (2011).
[6] J. A. Sobota, S.-L. Yang, D. Leuenberger, A. F. Kemper, J. G. Analytis, I. R. Fisher, P. S. Kirchmann, T. P. Devereaux, and Z.-X. Shen, Phys. Rev. Lett. **113**, 157401 (2014).
[7] K. M. F. Shahil, M. Z. Hossain, D. Teweldebrhan, and A. A. Balandin, Appl. Phys. Lett. **96**, 153103 (2010).
[8] Y. R. Shen, Nature (London) **337**, 519 (1989).
[9] M. Fiebig, V. V. Pavlov, and R. V. Pisarev, J. Opt. Soc. Am. B **22**, 96 (2005).
[10] I. I. Smolyaninov, A. V. Zayats, and C. C. Davis, Opt. Lett. **22**, 1592 (1997).
[11] Y. M. Chang, L. Xu, and H. W. K. Tom, Phys. Rev. Lett. **78**, 4649 (1997).
[12] H. B. Zhao, Y. Fan, G. Lüpke, A. T. Hanbicki, C. H. Li, and B. T. Jonker, Phys. Rev. B **83**, 212302 (2011).
[13] D. Hsieh, J. W. McIver, D. H. Torchinsky, D. R. Gardner, Y. S. Lee, and N. Gedik, Phys. Rev. Lett. **106**, 057401 (2011).
[14] D. Hsieh, F. Mahmood, J. W. McIver, D. R. Gardner, Y. S. Lee, and N. Gedik, Phys. Rev. Lett. **107**, 077401 (2011).
[15] R. Venkatasubramanian, E. Siivola, T. Colpitts, and B. O'Quinn, Nature (London) **413**, 597 (2001).
[16] W. Richter and C. R. Becker, Phys. Status Solidi B **84**, 619 (1977).
[17] W. Kullmann, J. Geurts, W. Richter, N. Lehner, H. Rauh, U. Steigenberger, G. Eichhorn, and R. Geick, Phys. Status Solidi B **125**, 131 (1984).
[18] A. Q. Wu, X. Xu, and R. Venkatasubramanian, Appl. Phys. Lett. **92**, 011108 (2008).
[19] Y. Wang, L. Guo, X. Xu, J. Pierce, and R. Venkatasubramanian, Phys. Rev. B **88**, 064307 (2013).
[20] J. Flock, T. Dekorsy, and O. Misochko, Appl. Phys. Lett. **105**, 011902 (2014).
[21] O. A. Aktsipetrov, I. M. Baranova, and Yu. A. Il'inskiĭ, Sov. Phys. JETP **64**, 167 (1986) [Zh. Eksp. Teor. Fiz. **91**, 287 (1986)].
[22] M. Hajlaoui, E. Papalazarou, J. Mauchain, G. Lantz, N. Moisan, D. Boschetto, Z. Jiang, I. Miotkowski, Y. P. Chen, A. Taleb-Ibrahimi, L. Perfetti, and M. Marsi, Nano Lett. **12**, 3532 (2012).
[23] V. Denisov, B. Mavrin, and V. Podobedov, Phys. Rep. **151**, 1 (1987).
[24] S. J. Cyvin, J. E. Rauch, and J. C. Decius, J. Chem. Phys. **43**, 4083 (1965).
[25] H. J. Zeiger, J. Vidal, T. K. Cheng, E. P. Ippen, G. Dresselhaus, and M. S. Dresselhaus, Phys. Rev. B **45**, 768 (1992).
[26] G. A. Garrett, T. F. Albrecht, J. F. Whitaker, and R. Merlin, Phys. Rev. Lett. **77**, 3661 (1996).
[27] Y. D. Glinka, S. Babakiray, T. A. Johnson, M. B. Holcomb, and D. Lederman, Phys. Rev. B **91**, 195307 (2015).
[28] Y. D. Glinka, S. Babakiray, T. A. Johnson, and D. Lederman, J. Phys.: Condens. Matter **27**, 052203 (2015).